Supplement of Biogeosciences, 13, 5333–5355, 2016
http://www.biogeosciences.net/13/5333/2016/
doi:10.5194/bg-13-5333-2016-supplement

Biogeosciences
Open Access

Supplement of

Anaerobic oxidation of methane alters sediment records of sulfur, iron and phosphorus in the Black Sea

Matthias Egger et al.

Correspondence to: Matthias Egger (m.j.egger@uu.nl)

1 Multicomponent model formulation

Molecular diffusion coefficients D_m (cm^2 yr^{-1}) were corrected for tortuosity in the porous medium according to Boudreau (1996).

$$D' = \frac{D_m}{1 - 2\ln(\phi)}$$

To account for sediment compaction, a depth-dependent porosity (ϕ) was described by

$$\phi(x) = \phi_\infty + (\phi_0 - \phi_\infty)e^{-\frac{x}{\gamma}}$$

where x is the distance from the sediment-water interface (cm), ϕ_∞ the porosity at depth in the sediment, ϕ_0 the porosity at the sediment surface, and γ the porosity attenuation factor (see Fig. S1 and Table S1).

The advective velocity of solids at depth v_∞ was described by

$$v_\infty = \frac{F_{sed}}{\rho(1 - \phi_\infty)}$$

where F_{sed} denotes the sediment accumulation rate (g cm^{-2} yr^{-1}) and ρ the sediment density (Meysman et al., 2005).

2 Supplementary tables

Table S1. Environmental parameters used by the diagenetic model.

Parameter	Symbol	Value	Units
Porosity at surface	ϕ_0	0.97	-
Porosity at depth	ϕ_∞	0.61	-
Porosity e-folding distance	γ	95	cm
Sediment density	ρ	2.31	g cm^{-3}
Temperature	T	1	^{o}C
Bottom water Cl^- concentration*	$[Cl^-]_0$	$\frac{salinity}{1.80655 * M_{Cl^-} * \rho_{SW}}$	mol cm^{-3}
Bottom water SO_4^{2-} concentration*	$[SO_4^{2-}]_0$	$\frac{0.14 * salinity}{1.80655 * M_{SO_4^{2-}} * \rho_{SW}}$	mol cm^{-3}
C:N ratio of organic matter	C/N	6.625	-
C:P ratio of organic matter	C/P	106	-
C:P ratio of organic matter under anoxia	C/P_{anoxic}	424	
P:Fe ratio for $Fe(OH)_3^{\alpha}$	χ^{α}	0.1	-
P:Fe ratio for $Fe(OH)_3^{\beta}$	χ^{β}	0.055	-
P:Fe ratio for $Fe(OH)_3^{\gamma}$	χ^{γ}	0.03	-

*M_{Cl^-} and $M_{SO_4^{2-}}$ denote the molecular weights of Cl^- and SO_4^{2-}; ρ_{SW} is the seawater density calculated for the in-situ salinity, temperature and pressure.

Table S2. Mass balances for chemical species included in the diagenetic model (based on Tables 2 and 3)

$\frac{\partial OM^{\propto}}{\partial t} =$	$-\nu \frac{\partial OM^{\alpha}}{\partial x} - R1^{\alpha} - R2^{\alpha} - R3^{\alpha} - R4^{\alpha} - R5^{\alpha}$
$\frac{\partial OM^{\beta}}{\partial t} =$	$-\nu \frac{\partial OM^{\beta}}{\partial x} - R1^{\beta} - R2^{\beta} - R3^{\beta} - R4^{\beta} - R5^{\beta}$
$\frac{\partial OM^{\gamma}}{\partial t} =$	$-\nu \frac{\partial OM^{\gamma}}{\partial x}$
$\frac{\partial Fe(OH)_3{}^{\propto}}{\partial t} =$	$-\nu \frac{\partial Fe(OH)_3{}^{\propto}}{\partial x} - 4R3^{\alpha,\beta} + 4rR8 - 2R13 - 8R20^{\alpha} - R21$
$\frac{\partial Fe(OH)_3{}^{\beta}}{\partial t} =$	$-\nu \frac{\partial Fe(OH)_3{}^{\beta}}{\partial x} - 2R14 - 8R20^{\beta} + R21 - R22$
$\frac{\partial Fe(OH)_3{}^{\gamma}}{\partial t} =$	$-\nu \frac{\partial Fe(OH)_3{}^{\gamma}}{\partial x} + R22$
$\frac{\partial FeS}{\partial t} =$	$-\nu \frac{\partial FeS}{\partial x} - R9 + rR15 - R16 - R18 + R25 + 3R26$
$\frac{\partial FeS_2}{\partial t} =$	$-\nu \frac{\partial FeS_2}{\partial x} - 2R10 + R16 + R18$
$\frac{\partial FeCO_3}{\partial t} =$	$-\nu \frac{\partial FeCO_3}{\partial x} + rR24 - R25$
$\frac{\partial S_0}{\partial t} =$	$-\nu \frac{\partial S_0}{\partial x} + R13 + R14 - 4R17 - R18$
$\frac{\partial Fe_{ox}P}{\partial t} =$	$-\nu \frac{\partial Fe_{ox}P}{\partial x} - \chi^{\alpha}(4R3^{\alpha,\beta} - 4rR8 + 2R13 + 8R20^{\alpha}) - \chi^{\beta}(2R14 + 8R20^{\beta}) - (\chi^{\alpha} - \chi^{\beta})R21 - (\chi^{\beta} - \chi^{\gamma})R22$
$\frac{\partial Fe_3(PO_4)_2}{\partial t} =$	$-\nu \frac{\partial Fe_3(PO_4)_2}{\partial x} + rR23 - R26$
$\frac{\partial P_{org}}{\partial t} =$	$-\nu \frac{\partial P_{org}}{\partial x} - \frac{1}{106}(R1^{\alpha,\beta} + R2^{\alpha,\beta} + R3^{\alpha,\beta} + R4^{\alpha,\beta} + R5^{\alpha,\beta})$
$\frac{\partial CaP}{\partial t} =$	$-\nu \frac{\partial CaP}{\partial x}$
$\frac{\partial DetrP}{\partial t} =$	$-\nu \frac{\partial DetrP}{\partial x}$
$\frac{\partial Cl^-}{\partial t} =$	$D' \frac{\partial^2 Cl^-}{\partial x^2} - u \frac{\partial Cl^-}{\partial x}$
$\frac{\partial O_2}{\partial t} =$	$D' \frac{\partial^2 O_2}{\partial x^2} - u \frac{\partial O_2}{\partial x} - qR1^{\alpha,\beta} - 2R7 - R8 - 2qR9 - 7qR10 - 2R11 - 2R12$
$\frac{\partial SO_4^{2-}}{\partial t} =$	$D' \frac{\partial^2 SO_4^{2-}}{\partial x^2} - u \frac{\partial SO_4^{2-}}{\partial x} - \frac{1}{2} qR4^{\alpha,\beta} + qR9 + 4qR10 + R11 + qR17 - R19$
$\frac{\partial Fe^{2+}}{\partial t} =$	$D' \frac{\partial^2 Fe^{2+}}{\partial x^2} - u \frac{\partial Fe^{2+}}{\partial x} + 4qR3^{\alpha,\beta} - 4R8 + qR9 + 2qR10 + 2q(R13 + R14) - R15 + 8qR20^{\alpha,\beta} - 3R23 - R24$
$\frac{\partial H_2S}{\partial t} =$	$D' \frac{\partial^2 H_2S}{\partial x^2} - u \frac{\partial H_2S}{\partial x} + \frac{1}{2} qR4^{\alpha,\beta} - R11 - q(R13 + R14) - R15 - qR16 + 3qR17 + R19 - qR25 - 3qR26$
$\frac{\partial CH_4}{\partial t} =$	$D' \frac{\partial^2 CH_4}{\partial x^2} - u \frac{\partial CH_4}{\partial x} + \frac{1}{2} qR5^{\alpha,\beta} + R6 - R12 - R19 - qR20^{\alpha,\beta}$
$\frac{\partial NH_4^+}{\partial t} =$	$D' \frac{\partial^2 NH_4^+}{\partial x^2} - u \frac{\partial NH_4^+}{\partial x} + \frac{16}{106} q(R1^{\alpha,\beta} + R2^{\alpha,\beta} + R3^{\alpha,\beta} + R4^{\alpha,\beta} + R5^{\alpha,\beta}) - R7$
$\frac{\partial NO_3^-}{\partial t} =$	$D' \frac{\partial^2 NO_3^-}{\partial x^2} - u \frac{\partial NO_3^-}{\partial x} - \frac{4}{5} q(R2^{\alpha,\beta}) + R7$
$\frac{\partial HPO_4^{2-}}{\partial t} =$	$D' \frac{\partial^2 HPO_4^{2-}}{\partial x^2} - u \frac{\partial HPO_4^{2-}}{\partial x} - \frac{1}{106} q(R1^{\alpha,\beta} + R2^{\alpha,\beta} + R3^{\alpha,\beta} + R4^{\alpha,\beta} + R5^{\alpha,\beta}) + \chi^{\alpha}(4qR3^{\alpha,\beta} - 4R8 + 2qR13 + 8qR20^{\alpha}) + \chi^{\beta}(2qR14 + 8qR20^{\beta}) + q(\chi^{\alpha} - \chi^{\beta})R21 + q(\chi^{\beta} - \chi^{\gamma})R22 - 2R23 + 2qR26$
$\frac{\partial DIC}{\partial t} =$	$D' \frac{\partial^2 DIC}{\partial x^2} - u \frac{\partial DIC}{\partial x} + q(R1^{\alpha,\beta} + R2^{\alpha,\beta} + R3^{\alpha,\beta} + R4^{\alpha,\beta}) + \frac{1}{2} qR5^{\alpha,\beta} - R6 + R12 + R19 + qR20^{\alpha,\beta} - R24 + qR25$

$q = \frac{(1-\phi)}{\phi}$ and $r = \frac{\phi}{(1-\phi)}$ are used for unit conversion between solids and solutes

Table S3. Time-dependent boundary conditions at the sediment surface.

Parameter	$t > 9000\ yrs\ B.P.$	$9000 > t > 7600 yrs\ B.P.$	$t < 7600\ yrs\ B.P.$
J_{FeCO_3}	3.81	1.14	1.14
J_{S_0}	0	0	0
J_{CaP}	0.18	0.18	0.18
J_{DetrP}	0.32	0.095	0.095
$[O_2]$	0.18	0.18	0
$[Fe^{2+}]$	0	0	0
$[\sum H_2S]$	0	0	0.08
$[CH_4]$	0	0	0
$[\sum NH_4^+]$	0	0	0
$[NO_3^-]$	0	0	0
$[HPO_4^{2-}]$	0	0	0
$[DIC]$	3	3	3

Fluxes have units of mmol m^{-2} yr^{-1} and concentrations are in mmol L^{-1}. yrs B.P. = years before present.

3 Supplementary figures

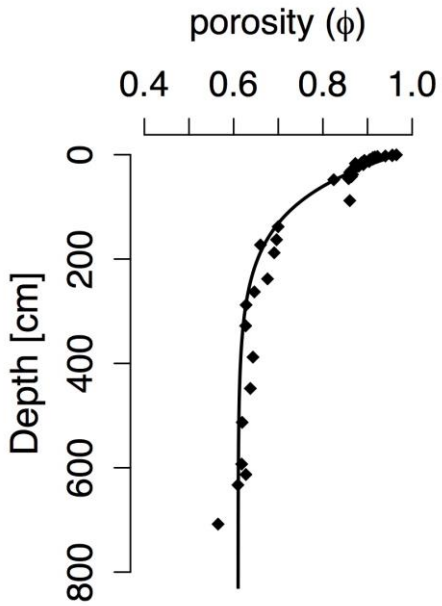

Figure S1. Porosity measurements (black diamonds) and modeled porosity profile (black line) at site 4.

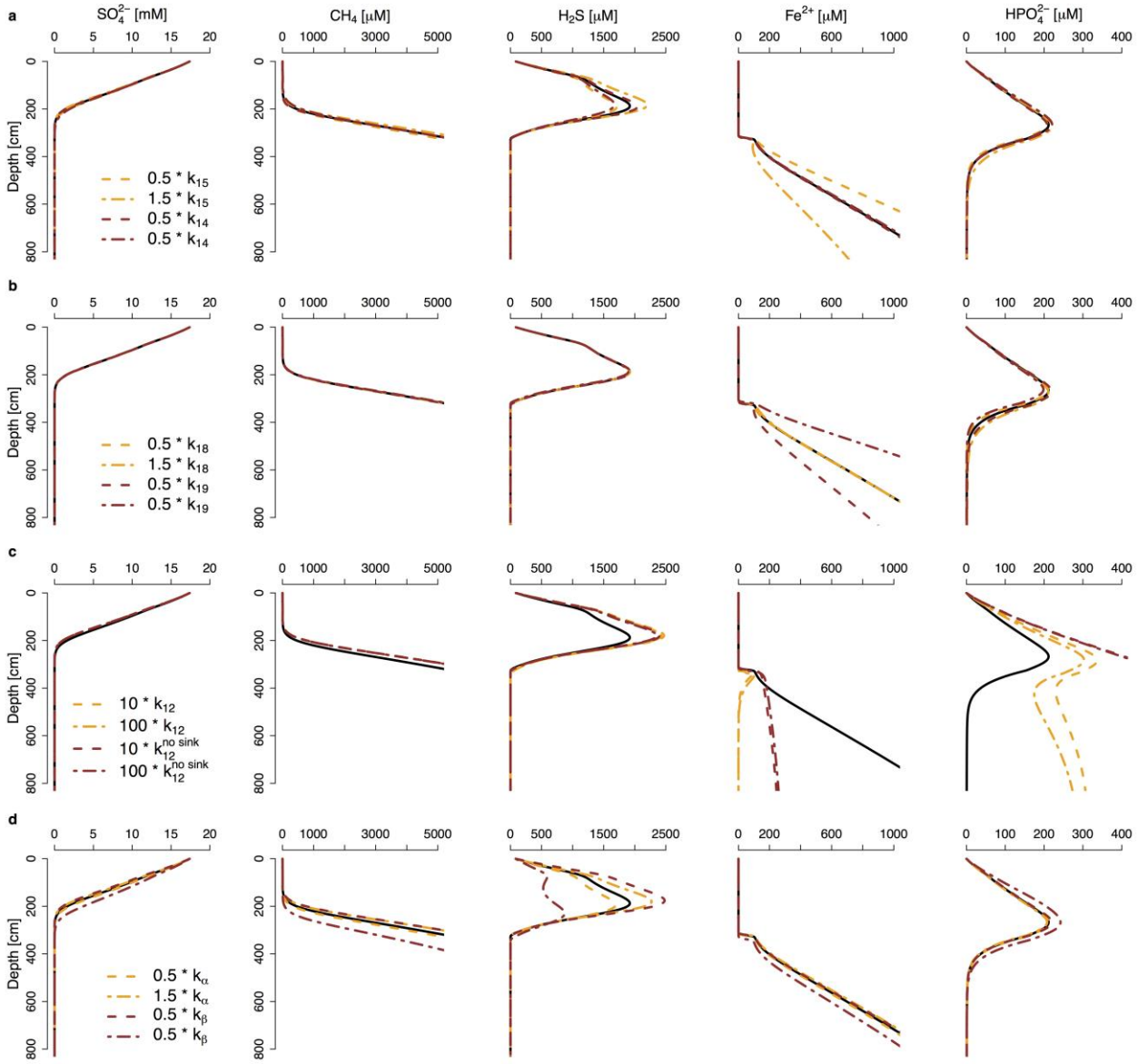

Figure S2. Sensitivity of modeled pore water profiles to changes in key parameters (see Table 4 and 5 for reaction equations and k values). The solid black lines represent the standard model run. (a) ± 50 % change in the rate constant for Fe-AOM (k_{15}, orange) and SO_4-AOM (k_{14}, brown). Note that the relative contribution of Fe-AOM to total AOM (i.e. sum of Fe-AOM and SO_4-AOM) varies between 0.4 to 0.9 % for the parameter range considered here. (b) ± 50 % change in vivianite (k_{18}, orange) and Fe carbonate (k_{19}, brown) formation rate constants. (c) 10 fold and 100 fold increase in S_0 disproportionation rate constant (k_{12}) and its effect on pore water profiles with (orange) and without (brown) sinks for dissolved Fe^{2+} (i.e. Fe(II) mineral formation). (d) ± 50 % change in decay constants for OM^{α} (k_{α}, orange) and OM^{β} (k_{β}, brown). In general, modeled profiles of sulfide, Fe^{2+} and HPO_4^{2-} show the highest sensitivity to the parameterization used.

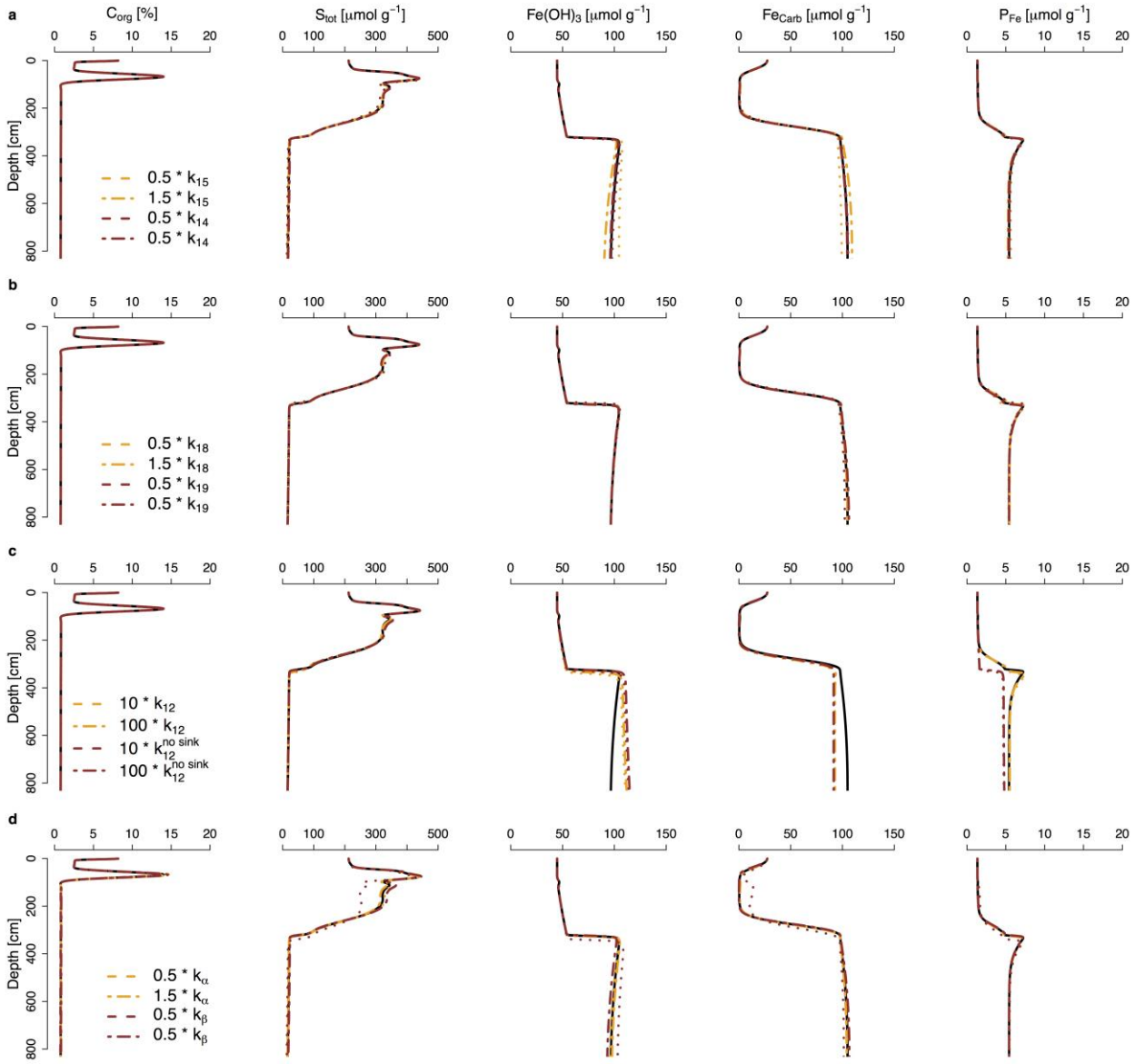

Figure S3. Sensitivity of modeled solid phase profiles to changes in key parameters (see Table 4 and 5 for reaction equations and k values). The solid black lines represent the standard model run. (a) ± 50 % change in the rate constant for Fe-AOM (k_{15}, orange) and SO_4-AOM (k_{14}, brown). (b) ± 50 % change in vivianite (k_{18}, orange) and Fe carbonate (k_{19}, brown) formation rate constants. (c) 10 fold and 100 fold increase in S_0 disproportionation rate constant (k_{12}) and its effect on pore water profiles with (orange) and without (brown) sinks for dissolved Fe^{2+} (i.e. Fe(II) mineral formation). (d) ± 50 % change in decay constants for OM^{α} (k_{α}, orange) and OM^{β} (k_{β}, brown). Note that the solid phase results are not very sensitive to the parameterization used.

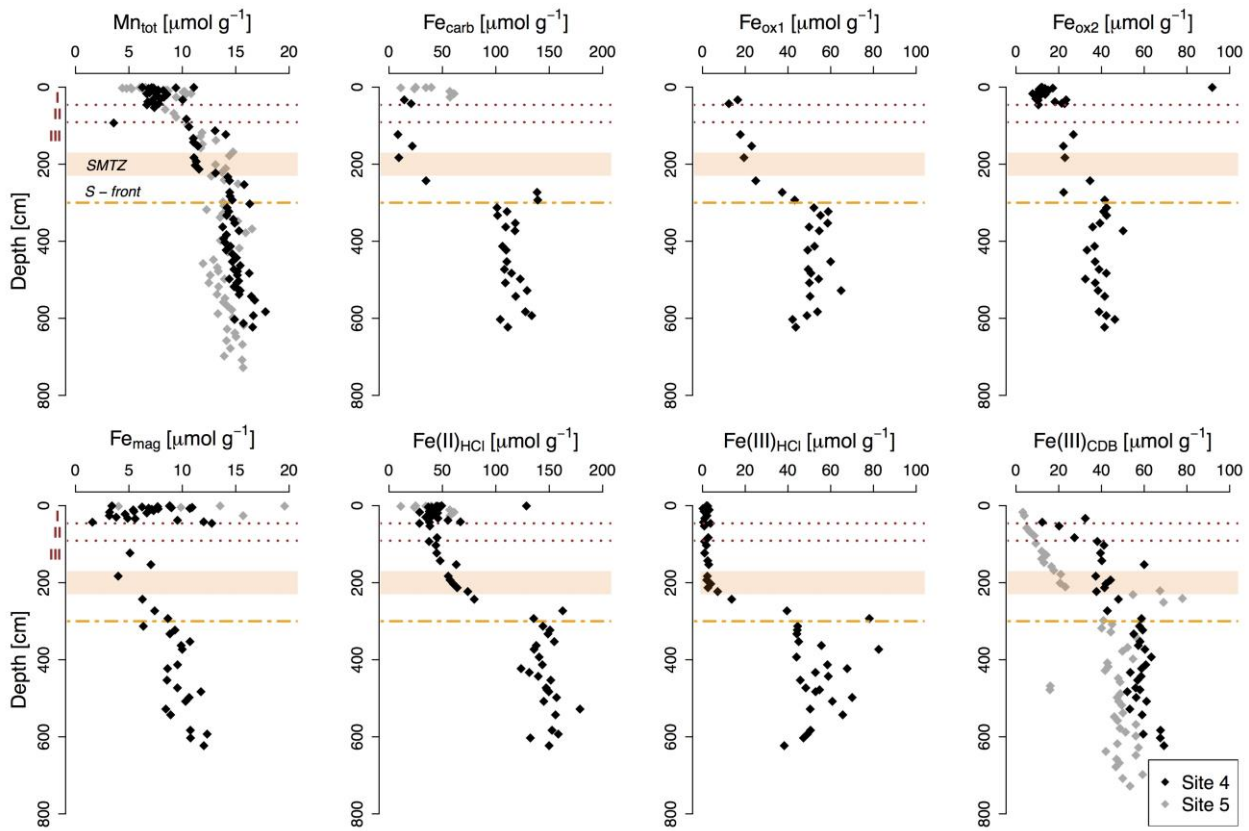

Figure S4. Solid phase profile of total sedimentary Mn and Fe extraction results for site 4 (black diamonds) and 5 (grey diamonds). See Table 1 for a description of the different Fe phases. Note that Fe_{carb} is not corrected for dissolution of AVS during the Na acetate extraction step. $Fe(III)_{CDB}$ for site 5 represents the amount of Fe extracted during the CDB-step of the SEDEX P extraction. Red dotted lines and roman numbers indicate the transitions between the lithological Unit I (modern coccolith ooze), Unit II (marine sapropel) and Unit III (limnic deposits). The orange bar represents the sulfate-methane transition zone (SMTZ) and the orange dashed line shows the current position of the downward migrating sulfidization front (S-front).

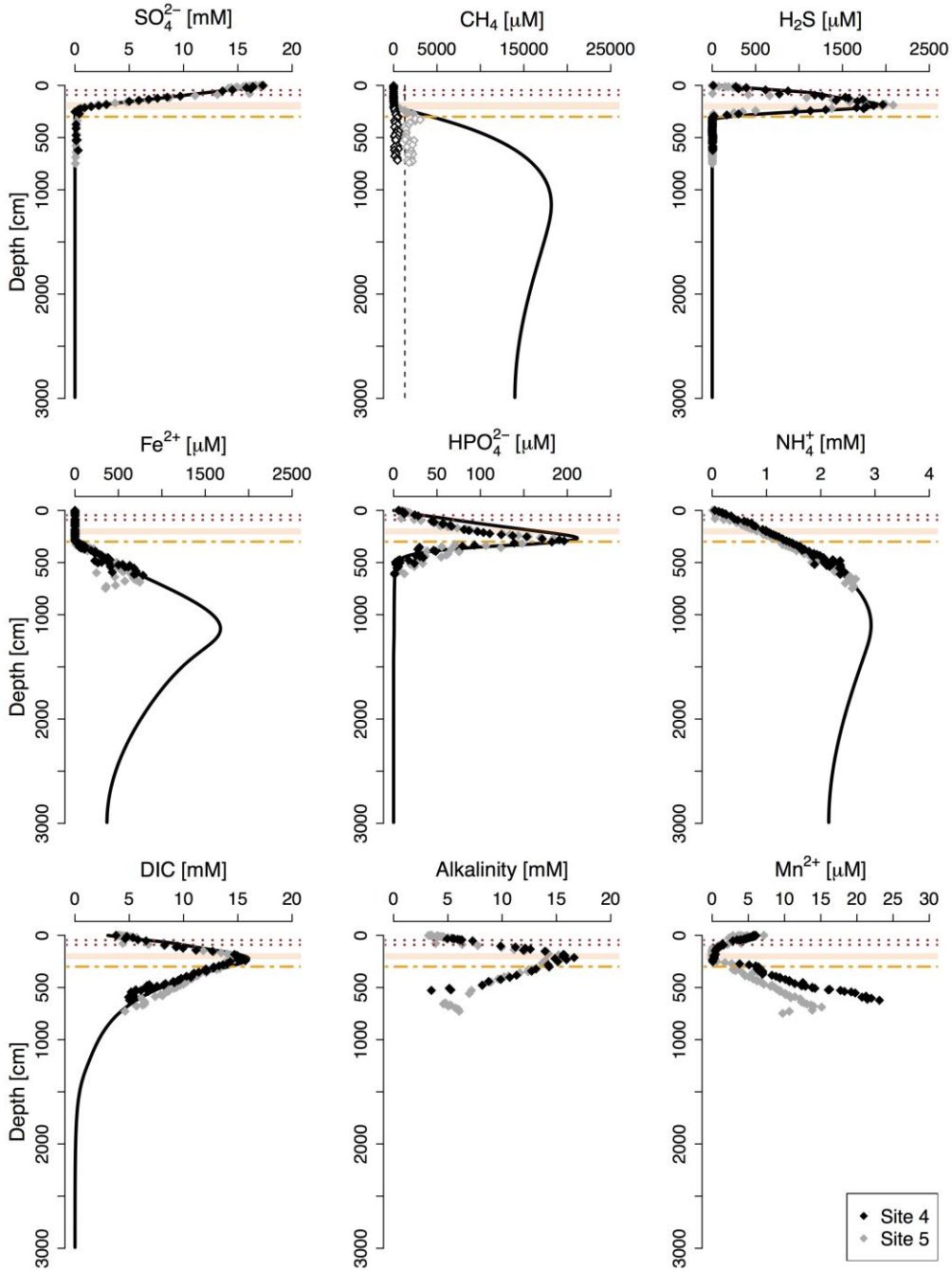

Figure S5. Pore water profiles (whole model domain, i.e. 3000 cm) for site 4 (black diamonds) and 5 (grey diamonds). Black lines represent profiles derived from the diagenetic model. Red dotted lines indicate the transitions between the lithological Unit I (modern coccolith ooze), Unit II (marine sapropel) and Unit III (limnic deposits). The orange bar represents the sulfate-methane transition zone (SMTZ) and the orange dashed line shows the current position of the downward migrating sulfidization front. The dashed vertical line indicates the CH_4 saturation concentration at atmospheric pressure (Mogollón et al., 2013). The open diamonds indicate CH_4 concentrations that are likely underestimated due to outgassing of CH_4 during coring.

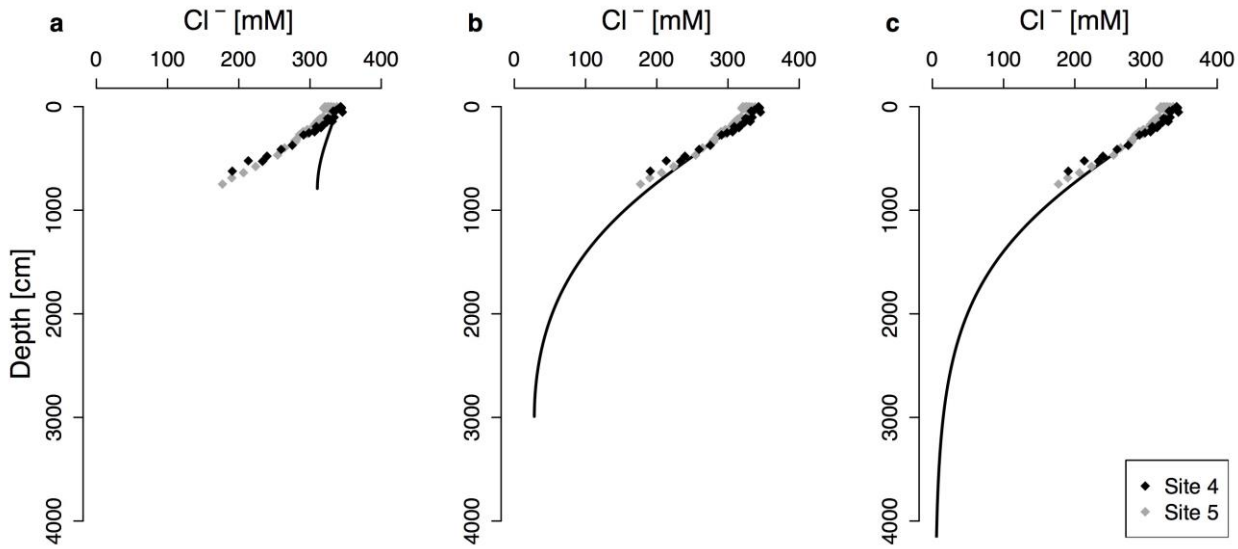

Figure S6. The influence of a zero gradient boundary condition at the base of the model domain on the pore water profile of chloride (Cl^-) is dependent on the modeled sediment depth. (a) Due to the transient diagenesis, a zero gradient is not reached within the depth range of the available data, i.e. the upper 800 cm. (b) A model length of 3000 cm results in a good fit of the modeled Cl^- profile with the measured pore water concentrations. Expanding the model domain to 4000 cm (c) largely increases the modeling time, with no significant improvement of the model fit. Thus, a depth range of 3000 cm was chosen in this study. The solid lines represent model simulations assuming an initial salinity of 1 for the freshwater phase and a linear increase to a salinity of 22 between 8500 and 1500 years ago, after which salinity stays constant.

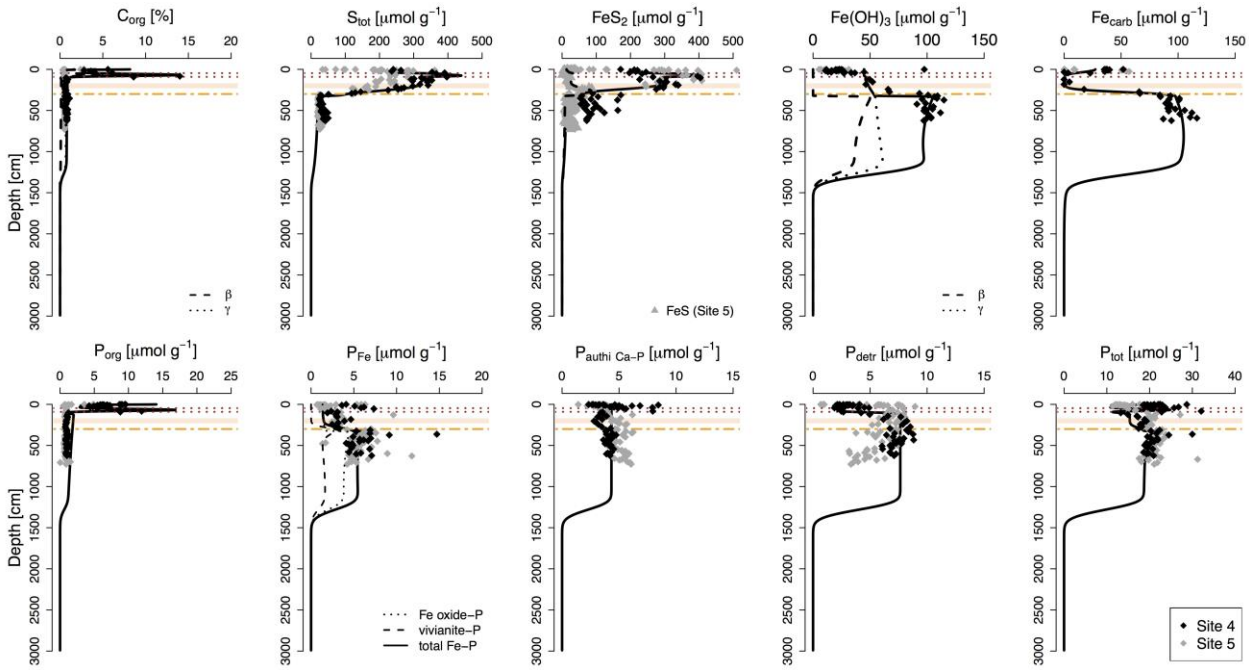

Figure S7. Solid phase profiles (whole model domain, i.e. 3000 cm) for site 4 (black diamonds) and 5 (grey diamonds). Fe_{carb} was corrected for apparent AVS dissolution during the Na acetate extraction step (the uncorrected Fe_{carb} data is given in Fig. S4). Black lines represent profiles derived from the diagenetic model. Red dotted lines indicate the transitions between the lithological Unit I (modern coccolith ooze), Unit II (marine sapropel) and Unit III (limnic deposits). The orange bar represents the sulfate-methane transition zone (SMTZ) and the orange dashed line shows the current position of the downward migrating sulfidization front.

Supplementary references

Boudreau, B. P.: The diffusive tortuosity of fine-grained unlithified sediments, Geochim. Cosmochim. Acta, 60(16), 3139–3142, doi:10.1016/0016-7037(96)00158-5, 1996.

Meysman, F. J. R., Boudreau, B. P. and Middelburg, J. J.: Modeling reactive transport in sediments subject to bioturbation and compaction, Geochim. Cosmochim. Acta, 69(14), 3601–3617, doi:10.1016/j.gca.2005.01.004, 2005.

Mogollón, J. M., Dale, A. W., Jensen, J. B., Schlüter, M. and Regnier, P.: A method for the calculation of anaerobic oxidation of methane rates across regional scales: An example from the Belt Seas and The Sound (North Sea-Baltic Sea transition), Geo-Marine Lett., 33(4), 299–310, doi:10.1007/s00367-013-0329-z, 2013.